Pergamon

Int. J. Heat Mass Transfer. Vol. 37, Suppl. 1, pp. 19–30, 1994

0017–9310/94 $6.00 + 0.00

0017–9310(93)E0112–T

Laminar heat transfer in a rectangular duct with a non-Newtonian fluid with temperature-dependent viscosity

SEHYUN SHIN and YOUNG I. CHO
Department of Mechanical Engineering and Mechanics, Drexel University, Philadelphia, PA 19104, U.S.A.

Abstract—The present study investigates the effect of the temperature-dependent and shear-thinning viscosity of a non-Newtonian fluid on the behavior of the laminar heat transfer and friction coefficients in a 2 : 1 rectangular duct. The H1 thermal boundary condition, corresponding to an axially-constant heat flux and a peripherally-constant temperature, was adopted for a top-wall-heated configuration. The present numerical results of local Nusselt numbers for a polyacrylamide (Separan AP-273) solution show 70–300% heat transfer enhancement over those of a constant-property fluid and give excellent agreement with recent experimental results. The heat transfer enhancement from the heated top wall is due to an increased velocity gradient near the wall, which is attributed to the combined effect of the temperature-dependent and shear-thinning viscosity. Two new correlations for the friction factor and the local Nusselt numbers in the 2 : 1 rectangular duct are proposed; these correlations cover both thermally-developing and thermally-fully-developed regions. This study also proposes the use of a temperature-dependent shear-thinning fluid in a rectangular duct in the design of a liquid cooling module for the computer industry.

INTRODUCTION

IN THE study of convective heat transfer phenomena, it is common to assume that the thermo–physical properties of fluids are constant. However, when applied to practical heat transfer problems in which large temperature differences occur between the wall and fluid, the constant-property assumption could cause significant errors in the estimation of the heat transfer coefficient as well as the pumping requirement. This is because viscosities of most liquids vary with temperature, a fact which significantly influences both velocity and temperature profiles. Consequently, the heat transfer and friction coefficients will be different from those obtained with a constant-property fluid, whose viscosity is independent of temperature.

The study of the laminar flow and heat transfer behavior in a rectangular duct has become increasingly important as a result of the ongoing development of an advanced liquid cooling module for electronic packaging, which uses a number of rectangular channels. In the rectangular duct, temperature-dependent Newtonian fluids can yield a significant heat transfer enhancement associated with the temperature-dependent viscosity [1, 2]. In addition, Hartnett and his coworkers [3–5] showed significant heat transfer enhancements with non-Newtonian fluids in the rectangular duct, an interesting result which was not observed in a circular pipe flow. The objective of the present paper is to investigate the effects of both the temperature-dependent and the shear-thinning viscosity of a non-Newtonian fluid on the laminar friction and heat transfer behavior in an asymmetrically heated 2 : 1 rectangular duct.

BACKGROUND

The analytical investigation of the effect of property variations on heat transfer is a highly complicated task for various reasons. First of all, the magnitude of the variations of fluid properties with temperature differs from one fluid to another. For non-Newtonian fluids, viscosity also varies with shear rate. In spite of these difficulties, however, many analytical, numerical, and experimental studies appear in the literature [3–19]. In general, the variation of the transport properties with temperature results in the enhancement of heat transfer due to increased velocity and temperature gradients. The amount of the heat transfer enhancement critically depends on the type of duct geometry and thermal boundary condition (i.e. symmetric or asymmetric).

Two schemes for the correction of the temperature-dependent property are briefly introduced below. The *reference-temperature* method introduces a reference temperature at which the properties appearing in the non-dimensional groups (*Re*, *Pr*, *Nu*, etc.) may be evaluated in such a way that the constant-property results may be used to evaluate variable-property behavior. Typically, the reference temperature may be the film temperature between the wall and bulk temperatures. In the *property-ratio* method, all properties are evaluated at the bulk temperature, and then all of the variable-property effects are lumped into a function of the ratios of some pertinent property evaluated at the wall temperature to that property evaluated at the bulk temperature. McElligot *et al.* [20] reported that the property ratio was better than the reference temperature method for heat transfer analysis, while the latter method was preferable for friction factor analysis.

NOMENCLATURE

a	constant in the Arrhenius relationship, equation (1)
$\bar{C}_p$	(dimensional) specific heat of fluid
$\bar{D}_h$	(dimensional) hydraulic diameter
$\bar{E}$	activation energy of flow per mole
F	function introduced in equation (7)
f	fanning friction factor, $(-\mathrm{d}\bar{P}/\mathrm{d}\bar{z})/[2\bar{D}_h/(\bar{\rho}\bar{V}_{avg}^2)]$
$\bar{g}$	gravity
Gr_q	modified Grashof number, $\bar{g}\bar{\beta}\bar{q}''\bar{D}_h^4/\bar{K}_f$
Gz	Graetz number, $(Re\,Pr\,\bar{D}_h)/\bar{z}$
$\bar{h}$	(dimensional) space-averaged heat transfer coefficient
$\bar{k}_f$	(dimensional) thermal conductivity of fluid
$\bar{K}$	(dimensional) fluid consistency index
$\bar{K}_y$	(dimensional) modified consistency index introduced in equation (5)
n	exponent introduced in equation (8)
n'	flow behavior index for non-Newtonian fluids
Nu	Nusselt number, calculated at the heated top wall, $hD_h/\bar{k}_f$
$\bar{p}$	(dimensional) static pressure
p	non-dimensional static pressure, $\bar{P}/\frac{1}{2}\bar{\rho}\bar{V}_{avg}^2$
Pr	Prandtl number, $\bar{\eta}_{ref}\bar{C}_p/\bar{k}_f$
$\bar{q}''$	(dimensional) heat flux
$\bar{R}$	(dimensional) gas constant per mole
Re	Reynolds number, $(\bar{\rho}\bar{V}_{avg}\bar{D}_h)/\bar{\eta}_{ref}$
Ra_q	modified Rayleigh number, $Gr_q Pr$
$\bar{r}$	(dimensional) radial distance
$\bar{S}_r$	reduced shear rate introduced in equation (3)
T	non-dimensional temperature, $(\bar{T}-\bar{T}_i)/(q''\bar{D}_h/\bar{k}_f)$
$\bar{T}_i$	(dimensional) fluid inlet temperature
$\bar{T}_w$	(dimensional) wall temperature
$\bar{v}_z$	(dimensional) axial velocity
v_z	non-dimensional axial velocity, $\bar{v}_z/\bar{v}_{avg}$
$\bar{V}_{avg}$	(dimensional) average axial velocity
$\bar{x}$, $\bar{y}$	(dimensional) axes of Cartesian coordinate system
x, y	non-dimensional axes of Cartesian coordinate, $\bar{x}/\bar{D}_h$, $\bar{y}/\bar{D}_h$
x^*, y^*	non-dimensional lateral and vertical distances, $\bar{x}/\bar{x}_0$, $\bar{y}/\bar{y}_0$
$\bar{z}$	(dimensional) axial distance
z	non-dimensional axial distance, $\bar{z}/(\bar{D}_h\,Re\,Pr)$.

Greek symbols

$\bar{\beta}$	(dimensional) volumetric expansion of fluid
$\bar{\dot{\gamma}}$	(dimensional) shear rate, $\sqrt{(\frac{1}{2}(\bar{\dot{\gamma}}:\bar{\dot{\gamma}}))}$
$\dot{\gamma}$	non-dimensional shear rate for hydrodynamically developed flow, $[(\partial\bar{v}_z/\partial\bar{x})^2+(\partial\bar{v}_z/\partial\bar{y})^2]^{0.5}$
Γ	aspect ratio (i.e. ratio of width to height $= y_0/x_0$)
δ	ratio of the non-Newtonian to Newtonian shear rate, $(3n'+1)/4n'$
ζ	constant viscosity—variation parameter introduced in equation (14)
$\bar{\eta}_{ref}$	(dimensional) reference viscosity (at inlet temperature of 20°C)
η	non-dimensional viscosity, $\bar{\eta}(\bar{\dot{\gamma}})/\bar{\eta}_{ref}$
η_0	zero-shear rate viscosity, $\bar{\eta}(\bar{\dot{\gamma}})/\bar{\eta}_{ref}$
Θ	neighboring dependent variable introduced in equation (16)
λ	characteristic time
ξ	constant Deborah number–variation parameter in equation (14)
Ψ	correction factor for friction factor introduced in equation (7)
Ω	correction factor for Nusselt number introduced in equation (22).

Subscripts

b	bulk
cp	constant-property
CPF	constant-property fluid
f	film
i	inlet
o	unperturbed
TICF	temperature-independent Carreau fluid
vp.n'	variable-property for arbitrary n'
w	wall
z	axial direction.

Superscript

$\bar{}$	dimensional quantities.

Non-isothermal laminar flow in a circular pipe

The viscosity of a Newtonian fluid, μ, is traditionally related to temperature by the Arrhenius relationship [8]:

$$\mu = a\exp(\bar{E}/\bar{R}\bar{T}) \tag{1}$$

where $\bar{E}$ is the activation energy of flow per mole, $\bar{R}$ is the gas constant per mole, $\bar{T}$ is an absolute temperature, and a is a constant for a given fluid. Using this equation, the shear stress of the Newtonian fluid, $\bar{\tau}$, can be expressed as follows:

$$\bar{\tau} = a\exp(\bar{E}/\bar{R}\bar{T})(-\mathrm{d}\bar{v}/\mathrm{d}\bar{r}). \tag{2}$$

For a non-Newtonian fluid such as the power-law fluid, an analogous expression might be written as:

$$\bar{\tau} = \bar{k}_\sigma[\exp(\bar{E}/\bar{R}\bar{T})(-\mathrm{d}\bar{v}/\mathrm{d}\bar{r})]^{n'} = \bar{k}_\sigma \bar{S}_r^{n'}, \quad (3)$$

where the term $\bar{S}_r$ is the 'reduced shear rate', and $\bar{k}_\sigma$ is the fluid consistency index, both independent of temperature. This equation was used to modify the power-law model in order to include the temperature effect on non-Newtonian viscosity in the present study. Hanks and Christiansen [9] derived the following relationship between non-isothermal friction factor, f_{niso}, and flow rate, $\bar{Q}$:

$$f_{\mathrm{niso}} = \frac{\bar{\tau}_w}{\frac{1}{2}\bar{\rho}\bar{V}^2} = \bar{k}_\gamma[\bar{Q}/\pi\bar{r}^3]^{n'}\Psi^{-1}, \quad (4)$$

where

$$\bar{k}_\gamma = \bar{k}_\sigma\left(\frac{3n'+1}{4n'}\right)^{n'}\exp(n'\bar{E}/\bar{R}\bar{T}). \quad (5)$$

The subscript 'niso' represents non-isothermal, and Ψ is a non-isothermal flow function dependent on both flow behavior index, n', and temperature. Rearranging equation (4) and comparing it with the isothermal friction factor, f_{iso}, Hanks and Christiansen [9] obtained the following correlation:

$$f_{\mathrm{niso}}\Psi = f_{\mathrm{iso}} = \frac{16}{Re}. \quad (6)$$

The friction factor in a non-isothermal flow can be calculated from either equations (4) or (6), provided that Ψ can be evaluated. Hanks and Christiansen [9] proposed a procedure to obtain the correction factor for a non-isothermal friction factor, Ψ, as follows:

$$\Psi = \frac{3n'+1}{n'}F\exp[(1-n')(\bar{E}/\bar{R})(1/\bar{T}_i - 1/\bar{T}_w)], \quad (7)$$

where F is known as a function of the Graetz number.

Laminar heat transfer in a circular pipe flow

For a circular pipe flow, where a symmetric heating at the wall is expected, Sieder and Tate [6] experimentally investigated the effect of the variable viscosity of oils on heat transfer in both heating and cooling cases. The temperature effect on heat transfer was shown in the following equation:

$$Nu/Nu_{\mathrm{cp}} = (\eta_b/\eta_w)^n, \quad (8)$$

where η_b and η_w represent viscosities evaluated at local bulk and local wall temperatures, respectively, and Nu_{cp} represents the Nusselt number corresponding to a constant-property fluid. Sieder and Tate [6] reported that the n value in equation (8) was 0.14 for the laminar Newtonian fluid flow in a circular pipe.

Pigford [10] obtained a solution for both thermally-developing Newtonian and non-Newtonian (power-law) fluid flow by extending the Leveque's solution to include the effects of variable viscosity and buoyancy. His analysis for the constant wall temperature case in the form of Nu_T resulted in

$$Nu_T = 1.75\delta^{1/3}Gz^{1/3}, \quad (9)$$

where $\delta = \bar{\dot{\gamma}}_w/(8\bar{V}/\bar{D})$, and $\bar{\dot{\gamma}}_w$ is a function of Gz, η_b/η_w, and Gr. Physically, the term δ represents the ratio of the velocity gradient at the wall. Pigford [10] showed that δ is equal to $[(3n'+1)/4n']$ for power-law fluids. It is of note that the non-Newtonian effect has been taken into account by a simple multiplication of $[(3n'+1)/4n']^{1/3}$ to the corresponding Newtonian result.

In order to accommodate the effect of the viscosity–temperature dependence, Metzner *et al.* [11] added an empirical term, similar to that of Sieder–Tate, to equation (9) as follows:

$$Nu = 1.418\delta^{1/3}Gz^{1/3}(\bar{K}_b/\bar{K}_w)^n. \quad (10)$$

This equation allows the velocity profile to distort according to the viscosity variation with temperature. Christiansen and Craig [12] pointed out the limitation of this empirical correction term in equation (10) when n approaches zero in a plug flow.

Mizushina *et al.* [13] suggested a two-step temperature correction; one for the entrance region and the other for the thermally-fully-developed region. Bassett and Welty [14] conducted an experimental study of the laminar heat transfer behavior for aqueous solutions of carboxymethyl cellulose (CMC) and polyethylene oxide (Polyox). The viscosity of the Polyox solution showed greater pseudo-plasticity (with a smaller fluid behavior index, n') than the CMC solution, while the viscosity of the CMC solution depended on temperature more than the Polyox fluid. They concluded that the local wall shear rate controlled the heat transfer rate, and that the shear rate was more profoundly affected by the viscosity variation with temperature than by the pseudo-plasticity. Joshi and Bergles [15] experimentally studied the effects of non-Newtonian behavior and temperature-dependent fluid consistency index (K) on the heat transfer, and proposed two correlations to account for these two effects.

Cho and Hartnett [16] summarized the empirical correlations for the laminar heat transfer for non-Newtonian fluids and pointed out that, for a large bulk-to-wall temperature difference, the correlation should include the corrections for the temperature-dependent viscosity effect as well as for natural convection.

Table 1 summarizes some of the important empirical equations which considered temperature-dependence into the laminar heat transfer. In general, the fluid consistency index correction, $(K_b/K_w)^n$, for both entrance and fully-developed regions became a function of the power-law index, n'.

Laminar heat transfer in a non-circular duct

Turning to a non-circular duct geometry, Cochrane [17] numerically investigated the laminar heat transfer behavior of flow between two parallel plates using a temperature-dependent power-law model. Gingrich *et al.* [18] investigated the effects of shear-thinning vis-

Table 1. Empirical correlations for laminar heat transfer

References	Correlations
Constant heat flux:	
Mizushina *et al.* [13]	$Nu_x = 1.41\delta^{1/3}Gz^{1/3}\left[\frac{K_b}{K_w}\right]^{0.14/n^{0.7}}$
Bassett and Welty [14]	$Nu_x = 1.85Gz^{1/3-0.03\delta_w}$
Constant temperature:	
Pigford [10]	$Nu_{mean} = 1.75\delta^{1/3}Gz^{1/3}$
Metzner *et al.* [11]	$Nu_{mean} = 1.75\delta^{1/3}Gz^{1/3}\left[\frac{K_b}{K_w}\right]^{0.14}$
Gori [26]	$Nu_{mean} = 1.75\delta^{1/3}Gz^{1/3}\left[\frac{K_b}{K_w}\right]^{a}$ where $a = 0.14\frac{4}{\left[\frac{3n'+1}{n'}\right]^{n'}}$
Ghosh and Rao [27]	$Nu_{mean} = 1.75\left[Gz+4.88\times10^{-4}\left(Ra\frac{L}{D}\right)_w^{0.75}\right]^{1/3}\left[\frac{K_b(3n'+1)}{K_w 2(3n'-1)}\right]^{0.14}$ (for heating)

cosity and viscous dissipation on the laminar heat transfer in a 2 : 1 rectangular duct.

Hartnett and Kostic [4] experimentally observed much higher heat transfer coefficients with viscoelastic fluids (polyacrylamide, Separan AP-273) in a laminar flow through a 2 : 1 rectangular duct than those with Newtonian fluids at the same Rayleigh number. Xie and Hartnett [3] experimentally studied the laminar heat transfer performance of aqueous solutions of Carbopol-934 (polyacrylic acid) and Separan AP-273 in a 2 : 1 rectangular duct with a top-wall-heated thermal boundary condition (i.e. H1). The local Nusselt numbers from the heated top wall increased by approximately two to three times over the values of water, a phenomenon that they attributed to a secondary flow resulting from an asymmetric velocity profile associated with the viscoelasticity of the two fluids [3]. Recently, Gao [5] has numerically shown evidence of secondary motions in the laminar flow of viscoelastic fluids in rectangular ducts using the Reiner–Rivlin model. Although the effect of the secondary flow on the friction factor was negligible, the secondary flow has a major effect on the heat transfer for viscoelastic fluids in rectangular ducts. The Nusselt number calculated by Gao for the Reiner–Rivlin fluid was in good agreement with experimental results of Xie and Hartnett [3].

Temperature-dependent viscosity model

There have been some attempts to investigate the combined effect of temperature-dependent and shear-thinning viscosity of a non-Newtonian fluid on the laminar heat transfer enhancement in a non-circular duct. Shadid and Eckert [19] proposed a temperature-shifted Carreau model and numerically studied a viscous dissipation problem by using a high viscosity fluid in a pipe flow. Shin and Cho [21] introduced a temperature-dependent Carreau model based on the viscosity measurements of polyacrylamide (Separan AP-273) solution; they found that the zero-shear-rate viscosity of the Separan solution was very sensitive to temperature, whereas the infinite-shear-rate viscosity was almost independent of temperature. They also reported the variations of characteristic time constant, λ, fluid behavior index, n', and fluid consistency index, K, with temperature [21].

PROBLEM DESCRIPTION AND ASSUMPTIONS

Figure 1 shows a schematic diagram of the system under consideration. Fluid enters the duct with a fully-developed parabolic velocity profile and a uniform temperature T_i. This study adopts the H1 thermal boundary condition corresponding to axially constant heat flux and peripherally constant temperature (top

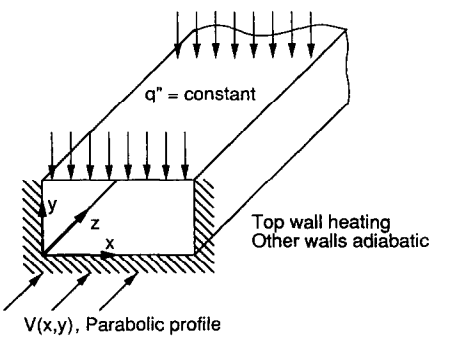

FIG. 1. Hydrodynamic and thermal boundary conditions. A developed velocity profile was used at the inlet of rectangular duct.

wall heated, and other walls adiabatic). In order to delineate the effect of the secondary flow at the corner of the rectangular duct, an axially-parallel flow was assumed such that the axial velocity, $v_z(x, y, z)$, was the only non-zero velocity component. Thus, the present calculation represents the case of a thermally-developing but axially-parallel flow with a heated top wall in the 2 : 1 rectangular duct. In other words, any heat transfer enhancement must be due to the changes in velocity and temperature gradients in the present calculation.

In order to simplify the computational model, the following treatments were incorporated.

1. Fluid properties are constant except for the viscosity which is dependent on the temperature and shear rate.
2. Axial conduction of thermal energy is negligibly small, which requires a large Peclet number (i.e. the product of the Reynolds number, Re, and the Prandtl number, Pr).
3. Viscous dissipation of thermal energy is negligibly small, which requires that the Brinkman number, Br, a measure of the magnitude of the viscous dissipation, be very small.
4. The term, $\eta(\dot{\gamma}, T)(\partial V_z/\partial z)$, in the axial momentum equation is negligibly small.

FORMULATION AND NUMERICAL TECHNIQUES

The non-dimensional forms of the conservation equations of mass, momentum, and energy for an axially parallel and thermally-developing flow in a rectangular duct are given as follows.

Continuity:

$$\int\int v_z(x, y)\,dx\,dy = 1.0. \tag{11}$$

Axial momentum:

$$\frac{\partial}{\partial x}\left(\eta(\dot{\gamma}, T)\frac{\partial v_z}{\partial x}\right)+\frac{\partial}{\partial y}\left(\eta(\dot{\gamma}, T)\frac{\partial v_z}{\partial y}\right) +2fRe_{\text{ref}} = 0. \tag{12}$$

Energy:

$$v_z(x, y)\frac{\partial T}{\partial z} = \left[\frac{\partial^2 T}{\partial x^2}+\frac{\partial^2 T}{\partial y^2}\right]. \tag{13}$$

The inlet temperature of 20°C is used as the reference temperature. In order to assess the role of viscosity variation on the development of the flow field due to temperature variation, the shear-thinning and temperature-dependent viscosity is employed by using the temperature-dependent Carreau model [21], which is given as

$$\frac{\eta(\dot{\gamma}, T)-\eta_\infty}{\eta_{0\,\text{ref}}10^{(\xi T)}-\eta_\infty} = [1+(De10^{\xi T}\dot{\gamma})^2]^{(n'-1)/2}. \tag{14}$$

In the above equation, De is the Deborah number $(\bar{\lambda}\bar{V}_{\text{avg}}/\bar{D}_h)$, ζ represents the slope of η_0 vs T curve, which becomes negative for heating case and positive for cooling case, and ξ is a constant accounting for the temperature dependence of time constant $(\bar{\lambda})$. T is a dimensionless temperature introduced for H1 boundary condition, defined as

$$T = \frac{(\bar{T}-\bar{T}_i)}{(\bar{q}''\bar{D}_h/\bar{k}_f)}. \tag{15}$$

Equation (14) considers the effects of temperature on the apparent viscosity, the time constant, and the fluid behavior index for a non-Newtonian fluid.

In the axial momentum equation, the product of the Fanning friction factor and the Reynolds number, fRe_{ref}, represents a source term. As mentioned earlier, the Reynolds number is based on the reference viscosity, η_{ref}, which is constant. In a non-isothermal flow, however, the local viscosity changes due to temperature. In this case, the physical meaning of fRe_{ref} should be carefully examined, as will be discussed later in Figs. 8(a) and (b).

Boundary conditions and solution methodology

Since detailed descriptions of the boundary conditions and the solution methodology have been given elsewhere [18, 23], only a brief summary is given below. The no-slip boundary condition is applied along the periphery of the duct for the axial velocity component. The constant heat flux boundary condition is applied only on the top wall of the rectangular duct. The other three walls are assumed to be adiabatic.

Solutions to the problem defined by the foregoing equations were obtained numerically by finite volume procedures [22]. A second-order accurate difference scheme was employed for the diffusion terms while the second-order upwinding scheme [23] was employed for the convective term in the energy equation for all interior nodal points. For the near-boundary control volumes, there was no need for a special discretization equation since the boundary condition data could be directly employed at the boundary face. This convenient property arose because the grid points were placed at the centers of the control volume. In the calculation of the rate of deformation tensor, a second-order central difference scheme was employed for the interior nodes, while a first-order difference between the near-boundary and boundary nodal points was employed for the near-boundary control volumes.

A fully implicit solution technique was adopted for both the momentum and energy equations at any given axial location. At a given axial location, the successive line under-relaxation (SLUR) procedure [24] was employed for the solution of the implicit finite difference form of the governing equations. Since the energy equation is parabolic in the axial direction, a marching solution was employed. For the momentum

equation, a predictor/corrector method was developed by employing SLUR for the inner iteration solver for a given fRe_{ref} product in combination with the Van Wijngaarden–Dekker–Brent searching methodology for the outer iteration [18].

Equations (12) and (13) were solved by an iterating procedure in which the temperature distribution obtained for constant-property assumption was used as the first approximation. Then, using the appropriate viscosity variation with temperature, as given in equation (14), the momentum equation was solved to yield the second approximation for the velocity distribution. This improved velocity distribution was employed in the calculation of the energy equation in order to yield the second approximation for the temperature distribution. The procedure was repeated until the velocity and temperature distributions changed less than 0.1%, as compared to the values from the previous step.

Convergence for the SLUR procedure was monitored by examining how well the discretization equation was satisfied by the current values of the dependent variables. For each grid point, the residual R was calculated as

$$r = \Sigma a_{nb}\Theta_{nb} + b - a_p\Theta_p, \qquad (16)$$

where Θ_{nb} are the neighboring dependent variables, a_{nb} are the coefficients corresponding to these neighboring dependent variables, b represents the other terms in the governing finite difference equations, Θ_p is the current nodal point dependent variable, and a_p is the coefficient corresponding to Θ_p. The convergence criteria for the SLUR method required that for any given grid point, the absolute value of the residual $|R|$ be less than 10^{-4}.

RESULTS AND DISCUSSION

The current numerical study used the viscosity data of an aqueous Polyacrylamide (Separan AP-273) solution reported by Shin and Cho [21]. The viscosity data shown in Fig. 2 were fitted using equation (14), and the maximum deviation between the measured viscosities and the predicted values from equation (14) was 4%.

Prior to presenting the present numerical solutions, we will assess the appropriate grid size for a constant-property fluid—a case in which well-established values of fRe_{ref} are available. On a uniform grid, we varied grid sizes and solved the continuity and momentum equations. The exact analytical value of fRe_{ref} in a fully-developed flow in a 2:1 rectangular duct is 15.54806; Shah and London's value is 15.55733; the corresponding value from the present study with 62×62 uniform grid was 15.52953. The values of fRe_{ref} became independent of grid sizes beyond 42×42. Hence, the present study used the results calculated from the 42×42 uniform grid size. Appropriate axial space-marching steps along the axial direction were chosen from 10^{-4} to 10^{-2} for the energy equation.

Figure 3 shows transport characteristic profiles on the mid-plane (i.e. $x^* = 0.5$), where $y^* = 1.0$ refers to the heated top wall, and $y^* = 0$ refers to the unheated bottom wall. Figure 3(a) shows the effect of the shear-thinning and temperature-dependent viscosity of the Separan solution on temperature profiles in a thermally-developing region, where two temperature profiles calculated for the Separan solution are compared with those for temperature-independent Carreau fluid (TICF) at two axial locations. Near the inlet (i.e. $z = 0.005$), there was not much difference between the two temperature profiles of the Separan solution and TICF. At $z = 0.05$, which was in the middle of the thermally-developing region, the temperature near the heated top wall for the Separan solution was much less than that for TICF. We believe that this phenomenon is due to an efficient heat removal caused by an increased velocity gradient near the heated top wall for the Separan solution.

Figure 3(b) shows the dimensionless viscosity profile of the Separan solution in the thermally-developing flow. At the inlet (i.e. $z = 0$), the viscosity of

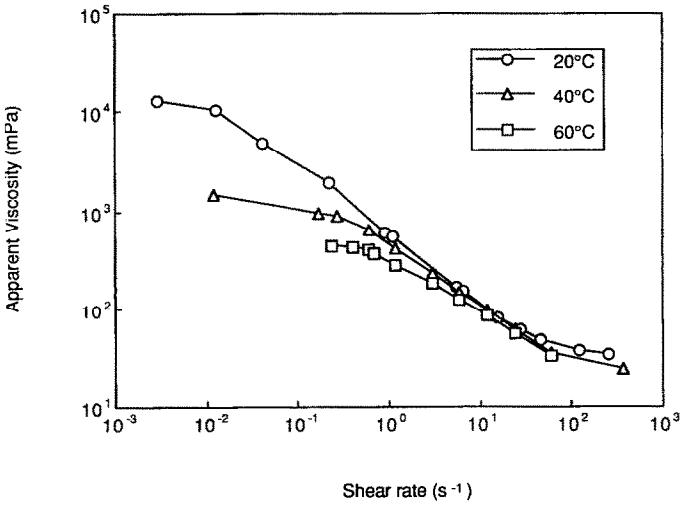

FIG. 2. Viscosities of the Separan solution (1000 w.p.p.m.) at three different temperatures with shear rate.

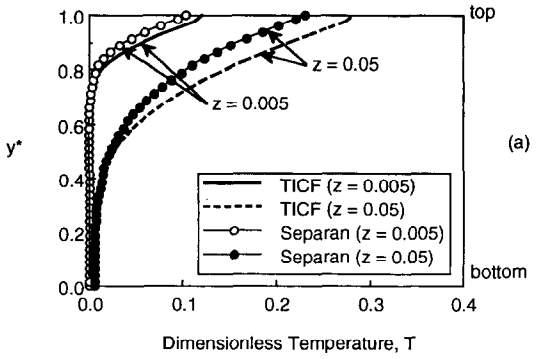

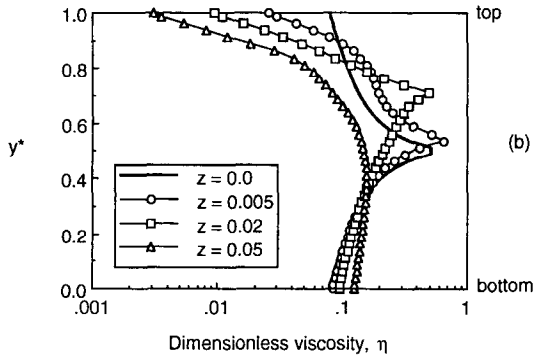

FIG. 3. (a) Dimensionless temperature profiles on mid-plane (i.e. $x^* = 0.5$) along the vertical (y) direction in a 2 : 1 rectangular duct with top-wall-heated, (b) dimensionless viscosity profiles on mid-plane (i.e. $x^* = 0.5$) along the vertical (y) direction in a 2 : 1 rectangular duct with top-wall-heated.

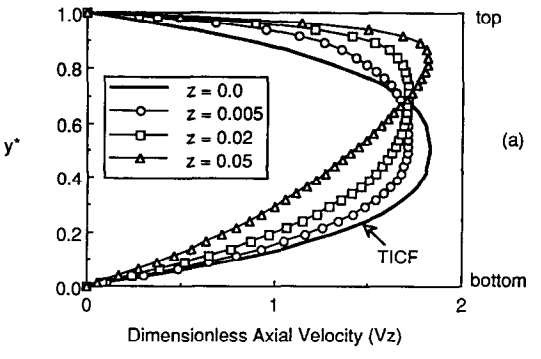

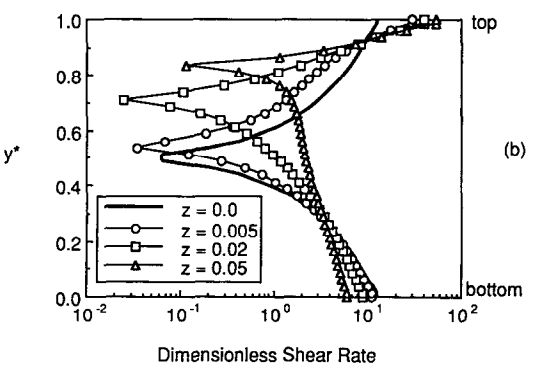

FIG. 4. (a) Dimensionless axial velocities on mid-plane (i.e. $x^* = 0.5$) along the vertical (y) direction in a 2 : 1 rectangular duct with top-wall-heated, and (b) dimensionless shear rates on mid-plane (i.e. $x^* = 0.5$) along the vertical (y) direction in a 2 : 1 rectangular duct with top-wall-heated.

the Separan solution was symmetric, as indicated by a thick solid line. The viscosity of the Separan solution near the heated top wall decreased dramatically with increasing axial distance (i.e. $\eta = 0.1$ at $z = 0$ to $\eta = 0.003$ at $z = 0.05$), while the viscosity at the bottom wall remained almost unchanged.

In order to delineate the effect of variable viscosity on velocity profiles in the thermally-developing flow field, Fig. 4(a) shows the velocity profiles at four different axial locations (i.e. $z = 0.0$, 0.005, 0.02, and 0.05). Obviously, the reduction of the viscosity caused a much steeper velocity gradient with increasing axial distance for the Separan solution than for the temperature-independent Carreau fluid (TICF). The fully-developed velocity profile for TICF (i.e. a thick solid curve, valid for all axial locations) is shown in Fig. 4(a) as a reference. The location of the maximum velocity for the Separan solution shifted from the center (i.e. $y^* = 0.5$) of the rectangular duct at the inlet toward the heated top wall with increasing axial distance.

Figure 4(b) shows the shear-rate profiles corresponding to the velocity profile at four different axial locations. The increase in the velocity gradient associated with the reduction of viscosity caused a high wall shear rate on the heated top wall. The location of the minimum shear rate moved toward the heated top wall in a manner similar to that of the maximum velocity.

The axial distributions of bulk and top-wall temperatures for the Separan solution and TICF are depicted in Fig. 5(a). The top wall temperature represents a space-averaged temperature. As a result of the increase in velocity gradients near the heated top wall, the wall temperatures for the Separan solution were much lower than those for TICF, and the bulk temperatures for the Separan solution were slightly higher than those for TICF.

Figure 5(b) shows the axial distribution of the wall and bulk temperature difference, $\Delta T_{\text{wall-bulk}}$, for the Separan solution and for TICF. It is noteworthy that a thermally-fully-developed flow is obtained when $\Delta T_{\text{wall-bulk}}$ reaches a plateau value. The results in Fig. 5(b) indicate that the thermal entrance length, L_{th^+}, for TICF is approximately $0.2 \sim 0.3$ in the top-wall-heated rectangular duct. The shear-thinning and temperature-dependent viscosity yielded much shorter thermal entrance lengths ($L_{\text{th}^+} = 0.05 \sim 0.07$) than for TICF.

Figure 6(a) presents the axial distributions of bulk, top-wall, and film viscosity for the Separan solution. The film viscosity was determined at film temperature and film shear rate. The present study used the film temperature that was first introduced by McAdams

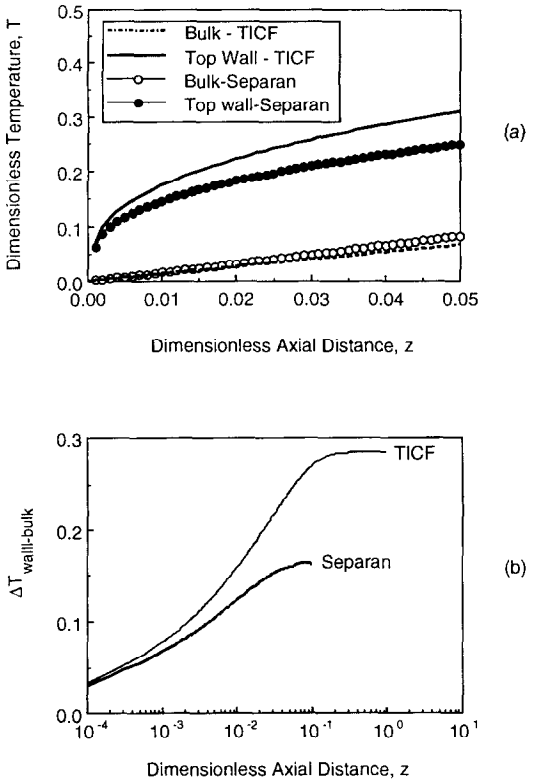

FIG. 5. (a) Dimensionless bulk and mean-wall temperature profiles along the dimensionless axial distance, z, (b) differential temperatures between wall and bulk, $\Delta T_{\text{wall-bulk}}$, along the dimensionless distance.

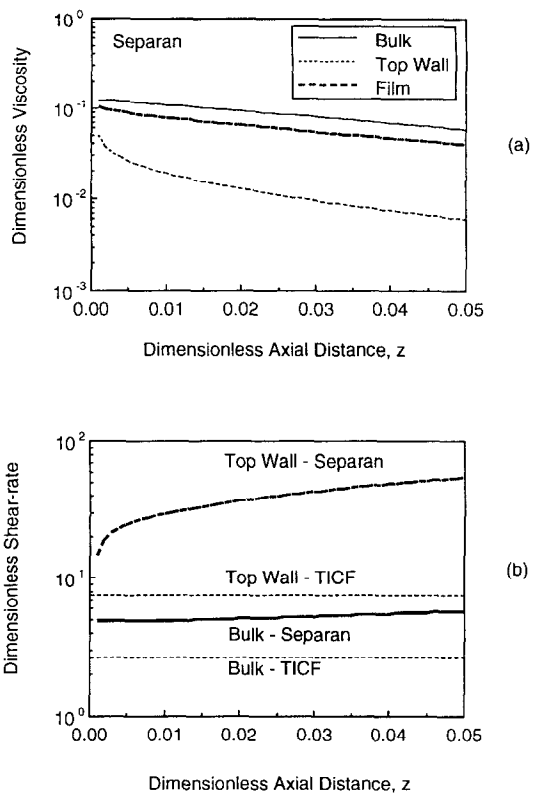

FIG. 6. (a) Dimensionless bulk and mean-wall viscosity profiles along the dimensionless axial distance, z, and (b) dimensionless bulk and mean-wall shear rate profiles along the dimensionless axial distance, z.

[25] as

$$T_f = T_b + \tfrac{1}{4}(T_w - T_b). \tag{17}$$

Similarly, we used the film shear rate, which was defined as

$$\dot{\gamma}_f = \frac{1}{4}\left(\frac{3}{\dot{\gamma}_b} + \frac{1}{\dot{\gamma}_w}\right)^{-1}. \tag{18}$$

Figure 6(b) shows the axial distributions of bulk and top-wall shear rates for the Separan solution and for TICF. The top-wall shear rate represents a space-averaged mean wall shear rate. Due to the increase of velocity gradients near the heated top wall, the top-wall shear rates for the Separan solution were much greater than those for TICF, and the bulk shear rates for the Separan solution were higher than those for TICF.

Figure 7(a) presents the ratio between the viscosity calculated at the top-wall temperature and that at the bulk fluid temperatures, η_w/η_b, along the axial direction. The viscosity ratios show constant values for both constant-property fluid (CPF) and TICF because the viscosity is independent of temperature in both cases. The viscosity ratio decreased for the Separan solution along the axial direction. Approaching the end of the thermal entrance length, the viscosity ratio for the Separan solution reached an asymptotic value, which depends on the magnitude of heat flux. The higher the heat flux is, the smaller the asymptotic value of the viscosity ratio is. Results in Fig. 7(a) indicate that a significant reduction in viscosity at any given axial location occurs as one moves from the center to the heated top wall of the rectangular duct along the transverse (i.e. y) direction.

In order to see the effect of the shear rate on the flow and heat transfer behavior, Fig. 7(b) shows the ratio of the bulk shear rate to the space-averaged top-wall shear rate, $\dot{\gamma}_b/\dot{\gamma}_w$, along the axial direction. The bulk shear rate is defined as follows:

$$\dot{\gamma}_b = \frac{\int \dot{\gamma} V_z \, dx\, dy}{\int V_z \, dx\, dy}. \tag{19}$$

Similar to the viscosity ratio, the ratios of the shear rate, $\dot{\gamma}_b/\dot{\gamma}_w$, for CPF and that for TICF showed constant values, whereas the corresponding shear rate ratio for the Separan solution decreased along the axial direction, reaching an asymptotic value for each heat flux.

Figure 8(a) shows the change in fRe_{ref} along the axial direction. At the inlet, fRe_{ref} had a value of 1.75

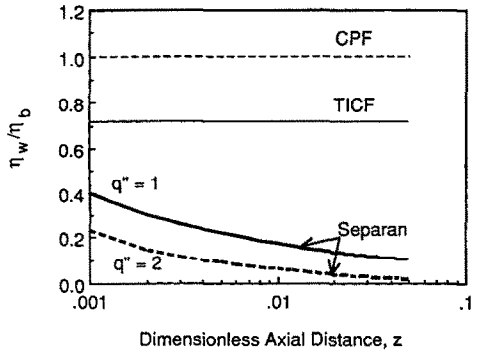

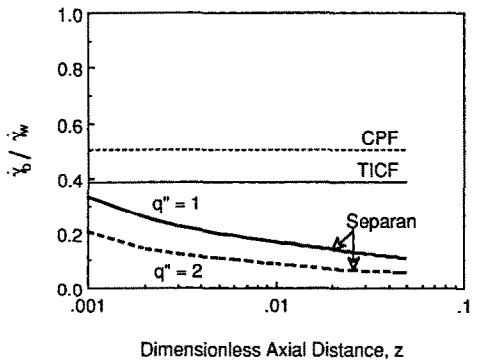

FIG. 7. (a) Viscosity ratio vs dimensionless axial distance, z and (b) shear rate ratio vs dimensionless axial distance, z.

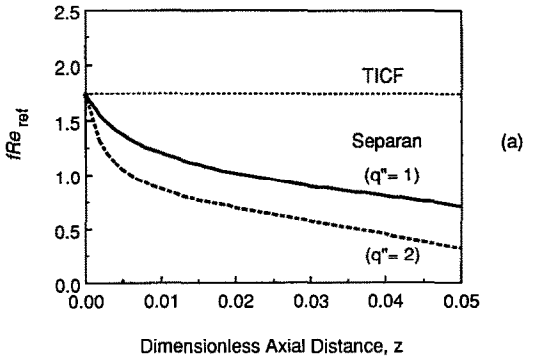

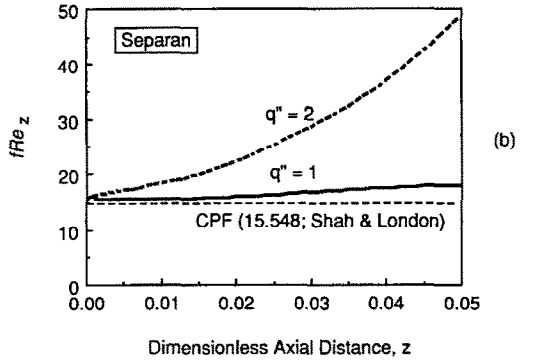

FIG. 8. (a) Product of the Fanning friction factor and the reference Reynolds number along the dimensionless axial distance, z, and (b) product of the Fanning friction factor and the local Reynolds number along the dimensionless axial distance, z.

for $n' = 0.65$ and $De = 100$. This value shows good agreement with the result of Gingrich *et al.* [18]. In the developing flow region, fRe_{ref} exponentially decreased with the axial distance. The higher the heat flux is, the more significantly fRe_{ref} decreases.

It is of note that fRe_{ref} is the dimensionless value of the axial pressure gradient $(-\Delta\bar{p}/\Delta\bar{z})$ in equation (12). From the definition of the friction factor, the axial pressure gradient might be expressed in terms of fRe as follows:

$$-\frac{\Delta p}{\Delta z} = f\frac{2\rho V_{avg}^2}{D_h} = f\frac{\rho V_{avg} D_h}{\eta}\left(\frac{2\eta V_{avg}}{D_h^2}\right)$$

$$= C_1 fRe_z \eta_z = C_1 fRe_{ref}\eta_{ref}. \quad (20)$$

The axial pressure gradient was proportional to the product of fRe_z and the local viscosity (η_z) evaluated at the local film temperature and shear rate. In a non-isothermal flow, the local Reynolds number (Re_z) is no longer constant because of the temperature dependency of viscosity. In order to obtain the local Reynolds number, the reference Reynolds number (Re_{ref}), evaluated at the zero-shear-rate viscosity (η_{ref}) at the reference temperature, should be corrected for the local film viscosity (η_f). In Fig. 8(b), the products of the friction factor and the local Reynolds number, fRe_z, are shown at two different heat fluxes. The local fRe_z increased along the axial direction, which can be attributed to the decrease of η_z as well as the skewed velocity profiles.

Figure 9 shows the ratio of the friction factor for the Separan solution to that for TICF, f/f_{TICF}, as a function of the film temperature, T_f. The subscript 'TICF' indicates a value for the temperature-independent Carreau fluid. In the thermally-developing region, the friction factor ratios correlate well with the following equation:

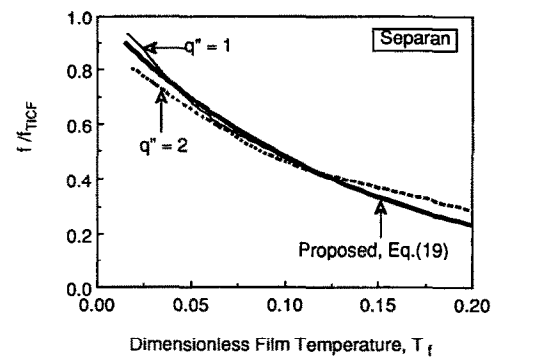

FIG. 9. The relative Fanning friction factor vs dimensionless film temperature.

$$\frac{f}{f_{\mathrm{TICF}}} = \frac{fRe_{\mathrm{ref}}}{fRe_{\mathrm{TICF}}} = [10^{-\zeta\tau_{\mathrm{f}}}]^{0.38}. \quad (21)$$

where fRe_{TICF} was given by Gingrich *et al.* [18].

In order to examine the effect of the variable viscosity on the laminar heat transfer for the Separan solution, local Nusselt numbers are shown at two different modified Rayleigh numbers (Ra_{q}) in Fig. 10(a), giving good agreement with experimental results for the Separan solution reported by Xie and Hartnett [3]. In the thermally-fully-developed region, the present calculation for TICF (with $n' = 0.65$) yielded a Nusselt number of 3.7, which is almost identical to the analytical value in a pipe flow ($Nu = \delta^{1/3} Nu_{\infty} = 3.69$).

Figure 10(b) presents the local Nusselt numbers against the Graetz number. The Nusselt number for the Separan solution increased by 70–300% above the value obtained with the constant-property fluid (CPF). We believe that the laminar heat transfer enhancement with the Separan solution occurs because of the decrease in the viscosity near the heated top wall, which brings out a significant increase in velocity gradients and subsequent decrease in fluid temperatures near the heated top wall, rendering the overall increase in the local heat convection performance. From the results given in Figs. 10(a) and (b), we conclude that the viscosity-variation parameter, ζ, and the amount of heat flux, q'', are directly related to the heat transfer enhancement for the Separan solution. In other words, the combined effect of the shear-thinning and temperature-dependent characteristics of the viscosity of the Separan solution causes 70–300% heat transfer enhancement in the 2 : 1 rectangular duct.

Figure 10(b) shows a tendency for an increasing Nusselt number near the end of exit of the rectangular duct (i.e. as the Graetz number decreases) particularly for the cases of high flux of $q'' = 2$, 3, and 5. It is speculated that the high heat flux at the top wall continues to decrease the fluid viscosity, thus increasing local Reynolds numbers as fluid approaches the exit. Hence, the Nusselt number does not show the usual asymptotic behavior with decreasing Graetz number. Instead, there is a slight tendency for an increasing Nusselt number approaching the exit of the rectangular duct for the cases of high heat flux.

The present study considers the viscosity ratio, $\eta_{\mathrm{w}}/\eta_{\mathrm{b}}$, as well as the shear-rate ratio, $\dot{\gamma}_{\mathrm{b}}/\dot{\gamma}_{\mathrm{w}}$, for the heat transfer correlation of non-Newtonian fluids. These two ratios may be combined into one, using the fluid consistency index. We propose a correction factor (Ω) for the Nusselt number in a non-isothermal laminar flow as follows:

$$Nu_{\mathrm{vp},n'} = \left(\frac{Nu_{\mathrm{vp},n'}}{Nu_{\mathrm{cp},n'}}\right)\left(\frac{Nu_{\mathrm{cp},n'}}{Nu_{\mathrm{cp},n'=1}}\right) Nu_{\mathrm{cp},n'=1}$$

$$= \Omega Nu_{\mathrm{cp},n'=1} \quad (22)$$

where the subscripts vp and cp represent the cases of variable-property and constant-property fluids with temperature. Also,

$$\Omega = \left(\frac{K_{\mathrm{b}}}{K_{\mathrm{w}}}\right)^{n} \delta^{1/3}$$

$$Nu_{\mathrm{cp},n'=1} = 1.35 Gz^{1/3} \quad (23)$$

where

$$n = 0.08\,(\log Gz - 2.5)^2 + 0.14. \quad (24)$$

Therefore, the proposed Nusselt number correlation becomes

$$Nu_{\mathrm{vp},n'} = \left(\frac{K_{\mathrm{b}}}{K_{\mathrm{w}}}\right)^{(0.08(\log Gz - 2.5)^2 + 0.14)} \times [(3n'+1)/4n']^{1/3}[1.35 Gz^{1/3}]. \quad (25)$$

Figure 11 shows the corrected Nusselt numbers in terms of Nu/Ω for CPF, TICF and the Separan solution. The corrected Nusselt numbers for the TICF and the Separan solution fall to the Nusselt number for the constant-property fluid, indicating that the laminar heat transfer coefficient for the TICF and the Separan solution can be predicted using equations

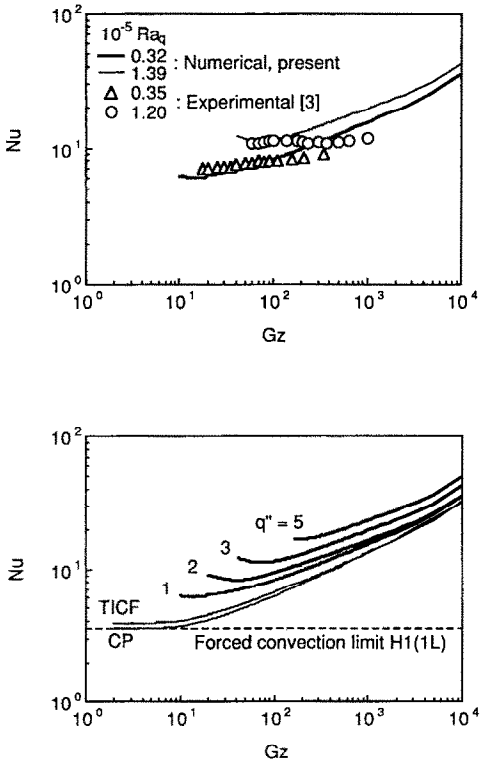

FIG. 10. (a) The comparison of the present numerical laminar heat transfer results of Separan with experimental results in a 2 : 1 rectangular duct with top-wall-heated. (b) Nusselt numbers for the Separan solution vs Graetz number at different heat fluxes.

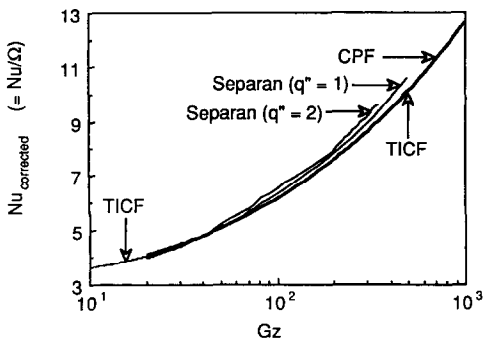

FIG. 11. The corrected Nusselt number vs Graetz number, *Gz*.

(22) or (25), provided that the temperature dependence of the fluid consistency index is known. For TICF, the first term in equation (22) is unity, and the only correction term is $\delta^{1/3}$. Meanwhile, for the Separan solution, the fluid consistency index ratio is included in equation (23) with $\delta^{1/3}$. The exponent, n, is 0.14 in the thermally-developing region and/or low heat flux case. In the case of a relatively high heat flux, the exponent, n, is strongly dependent on the Graetz number. Hence, we propose a new correlation of n, which depends on the Graetz number, as shown in equation (24). It is of note that the exponent, n, decreases with the Graetz number initially, and beyond a certain Graetz number, it starts to increase.

CONCLUSION

This study has conducted numerical calculations to examine the effect of the shear-thinning and temperature-dependent viscosity on the laminar heat transfer behavior in a top-wall-heated 2 : 1 rectangular duct, in which the effect of the secondary flow on the heat transfer was excluded. The present results of the local Nusselt numbers for the Separan solution showed excellent agreement with recent experimental results [3], and showed 70–300% enhancement over those of a constant-property fluid. The heat transfer enhancement occurred because of the steep velocity gradient occurring from the combined effect of shear-thinning and temperature-dependent viscosity. The present study proposes a new correlation for the friction factor and the laminar heat transfer at the heated top wall in the 2 : 1 rectangular duct; this correlation covers both thermally-developing and thermally-fully-developed regions. A temperature-dependent viscous fluid such as the Separan solution can be used for the purpose of the heat transfer enhancement in a liquid cooling module in electronic packaging, where uneven thermal boundary conditions with non-circular ducts are commonly utilized.

REFERENCES

1. C. Xie and J. P. Hartnett, Influence of variable viscosity of mineral oil on laminar heat transfer in a 2 : 1 rectangular duct, *Int. J. Heat Mass Transfer* **35,** 641–648 (1992).
2. S. Shin, Y. I. Cho, W. K. Gingrich and W. Shyy, Numerical study of laminar heat transfer with temperature dependent viscosity in a 2 : 1 rectangular duct, *Int. J. Heat Mass Transfer* **36,** 4365–4373 (1993).
3. C. Xie and J. P. Hartnett, Influence of rheology on laminar heat transfer to viscoelastic fluids, *Ind. Engng Chem. Res.* **31,** 727–732 (1992).
4. J. P. Hartnett and M. Kostic, Heat transfer to a viscoelastic fluid in laminar flow through a rectangular channel, *Int. J. Heat Mass Transfer* **28,** 1147–1155 (1985).
5. S. Gao, Flow and heat transfer of non-Newtonian fluids in a rectangular duct, Ph.D. Thesis, University of Illinois at Chicago (1993).
6. E. N. Sieder and G. E. Tate, Heat transfer and pressure drop of liquids in tubes, *Ind. Engng Chem.* **28**(12), 1429–1435 (1936).
7. A. H. P. Skelland, *Non-Newtonian Flow and Heat Transfer*. Wiley, New York (1967).
8. R. E. Gee and J. B. Lyon, Nonisothermal flow of viscous non-Newtonian fluids, *Ind. Engng Chem.* **49,** 956–960 (1957).
9. R. W. Hanks and R. G. Christiansen, The laminar nonisothermal flow of non-Newtonian fluids, *A.I.Ch.E. Jl* **7,** 519–523 (1961).
10. R. L. Pigford, Nonisothermal flow and heat transfer inside vertical tubes, *Chem. Engng Prog. Symp. Ser.* **51,** 79–92 (1955).
11. A. B. Metzner, R. D. Vaughn and G. L. Houghton, Heat transfer to non-Newtonian fluids, *A.I.Ch.E. Jl* **3,** 92–100 (1957).
12. E. B. Christiansen and S. E. Craig, Jr., Heat transfer to pseudoplastic fluids in laminar flow, *A.I.Ch.E. Jl* **8,** 154–160 (1962).
13. T. Mizushina, R. Ito, Y. Kuriwake and K. Yahikazawa, Boundary layer heat transfer in a circular tube to Newtonian and non-Newtonian fluids, *Kagaku Kogaku* **31,** 250–255 (1967).
14. C. E. Bassett and J. R. Welty, Non-Newtonian heat transfer in the thermal entrance region of uniformly heated horizontal pipes, *A.I.Ch.E. Jl* **21,** 691–706 (1975).
15. S. D. Joshi and A. E. Bergles, Experimental study of laminar heat transfer to in-tube flow of non-Newtonian fluids, *J. Heat Transfer* **102,** 397–401 (1980).
16. Y. I. Cho and J. P. Hartnett, Non-Newtonian fluids in circular pipe flow, *Adv. Heat Transfer* **15,** 59–141 (1982).
17. G. F. Cochrane, Jr., A numerical solution for heat transfer to non-Newtonian fluids with temperature-dependent viscosity for arbitrary condition of heat flux and surface temperature, Ph.D. Thesis, Oregon State University (1969).
18. W. K. Gingrich, Y. I. Cho and W. Shyy, Effect of shear thinning on laminar heat transfer behavior in a rectangular duct, *Int. J. Heat Mass Transfer* **35,** 2823–2836 (1992).
19. J. N. Shadid and E. R. G. Eckert, Viscous heating of a cylinder with finite length by a high viscosity fluid in steady longitudinal flow—II. Non-Newtonian Carreau model fluids, *Int. J. Heat Mass Transfer* **35,** 2739–2749 (1992).
20. D. M. McElligot, M. F. Taylor and F. Durst, Internal forced convection to mixtures of inert gases, *Int. J. Heat Mass Transfer* **20,** 475–486 (1977).
21. S. Shin and Y. Cho, Temperature effect on the viscosity of an aqueous polyacrylamide solution, *Int. Commun. Heat Mass Transfer* **20,** 831–844 (1993).
22. S. V. Patankar, *Numerical Heat Transfer and Fluid Flow*. Hemisphere, New York (1980).
23. W. Shyy, A study of finite difference approximations for

steady state, convection dominated flow problems, *J. Comput. Phys.* **57,** 415–438 (1985).
24. R. S. Varga, *Matrix Iterative Analysis.* Prentice-Hall, Englewood Cliffs, NJ (1962).
25. W. H. McAdams, *Heat Transmission.* Krieger, New York (1985).
26. F. Gori, Effects of variable physical properties in laminar flow of pseudoplastic fluids, *Int. J. Heat Mass Transfer* **21,** 247–250 (1977).
27. M. K. Ghosh and M. R. Rao, Heat transfer to non-Newtonian fluids in laminar flow in horizontal circular tubes, *Indian Chem. Engng* **14,** 33–38 (1972).